NeuroImage 200 (2019) 474–481

Contents lists available at ScienceDirect

NeuroImage

journal homepage: www.elsevier.com/locate/neuroimage

Shared and connection-specific intrinsic interactions in the default mode network

Jessica Samogin [a,1], Quanying Liu [a,b,c,d,1], Marco Marino [e], Nicole Wenderoth [a,b], Dante Mantini [a,e,*]

[a] Research Center for Motor Control and Neuroplasticity, KU Leuven, 3001, Leuven, Belgium
[b] Neural Control of Movement Laboratory, ETH Zurich, 8057, Zurich, Switzerland
[c] Division of Engineering and Applied Science, California Institute of Technology, Pasadena, United States
[d] Huntington Medical Research Institutes, Pasadena, United States
[e] Brain Imaging and Neural Dynamics Research Group, IRCCS San Camillo Hospital, 30126, Venice, Italy

ARTICLE INFO

Keywords:
Electroencephalography
Resting state
Functional connectivity
Time-frequency analysis
Neuronal communication
Intrinsic brain activity
Default mode network

ABSTRACT

Electrophysiological studies revealed that different neuronal oscillations, among which the alpha (8-13 Hz) rhythm in particular, but also the beta (13-30 Hz) and gamma (30-80 Hz) rhythms, are modulated during rest in the default mode network (DMN). Little is known, however, about the role of these rhythms in supporting DMN connectivity. Biophysical studies suggest that lower and higher frequencies mediate long- and short-range connectivity, respectively. Accordingly, we hypothesized that interactions between all DMN areas are supported by the alpha rhythm, and that the connectivity between specific DMN areas is established through other frequencies, mainly in the beta and/or gamma bands. To test this hypothesis, we used high-density electroencefalographic data collected in 19 healthy volunteers at rest. We analyzed frequency-dependent functional interactions between four main DMN nodes in a broad (1-80 Hz) frequency range. In line with our hypothesis, we found that the frequency-dependent connectivity profile between pairs of DMN nodes had a peak at 9-11 Hz. Also, the connectivity profile showed other peaks at higher frequencies, which depended on the specific connection. Overall, our findings suggest that frequency-dependent connectivity analysis may be a powerful tool to better understand how different neuronal oscillations support connectivity within and between brain networks.

1. Introduction

The default mode network (DMN) is a large-scale brain network comprising several brain regions, among which the posterior cingulate cortex (PCC), the medial prefrontal cortex (MPFC), and the left and right angular gyrus (LANG/RANG) have a primary role. Notably, the activity of the DMN at rest is typically higher than during performance of goal-directed tasks. For this reason, this network is considered the hallmark of the resting human brain (Buckner et al., 2008; Ganzetti and Mantini, 2013; Greicius et al., 2003; Raichle et al., 2001). The exact functions of the DMN are still a matter of debate, but there is mounting consensus concerning its involvement in spontaneous cognition and environment monitoring processes (Buckner et al., 2008; Buckner and Carroll, 2007; Mantini and Vanduffel, 2013).

The connectional properties of the DMN have been extensively investigated both at the structural and functional level using magnetic resonance imaging (MRI). MRI studies provided evidence for a hierarchical organization of the network into more specialized sub-networks (Andrews-hanna et al., 2010; Assaf et al., 2010; Chen et al., 2017; Hyatt et al., 2015; Uddin et al., 2009; Zhang et al., 2018). Generally speaking, the DMN has then been divided either into a ventral and a dorsal component or into a posterior and an anterior network, each including at least one of the four main DMN nodes (Andrews-hanna et al., 2010; Chen et al., 2017; Zhang et al., 2018).

A characterization of the brain rhythms contributing to DMN activity was performed by combining functional MRI (fMRI) with electroencephalography (EEG) (Mantini et al., 2007). Specifically, DMN activity measured using fMRI was correlated with band-limited EEG power variations in five frequency bands (delta, 1-4 Hz; theta, 4-8 Hz; alpha, 8-13 Hz; beta, 13-30 Hz; gamma, 30-50 Hz) (Mantini et al., 2007). This

* Corresponding author. Research Center for Motor Control and Neuroplasticity, KU Leuven Tervuursevest 101, 3001, Leuven, Belgium.
E-mail address: dante.mantini@kuleuven.be (D. Mantini).
[1] These authors contributed equally to this paper.

https://doi.org/10.1016/j.neuroimage.2019.07.007
Received 22 December 2018; Received in revised form 24 April 2019; Accepted 4 July 2019
Available online 4 July 2019

analysis revealed that the DMN has a specific electrophysiological signature involving the combination of different neuronal oscillations, and in particular the alpha and beta rhythms (Mantini et al., 2007). The importance of alpha and beta oscillations for mediating activity of DMN regions was suggested in recent studies based on electrocorticography (Hacker et al., 2017) and magnetoencephalography (MEG) data (Brookes et al., 2011; de Pasquale et al., 2010; Tang et al., 2017). By using MEG, the connectivity between PCC and MPFC, the posterior and anterior regions of the DMN respectively, was ascribed to neural oscillations in the alpha range (Tang et al., 2017). However, no study has been conducted to assess frequency-dependent connectivity between several DMN nodes. Since specific experimental conditions activate different sets of DMN nodes (Andrews-hanna et al., 2010; Uddin et al., 2009), it is conceivable that each sub-network is connected using one or more preferential frequencies.

In this study, we aim to test the hypothesis that EEG connectivity in the DMN largely depends on the frequency of neuronal oscillations considered. In particular, we postulate that alpha represents the carrier frequency supporting the connectivity across the whole network, whereas other frequency bands support the connectivity within DMN sub-networks. To test this hypothesis, we analysed high-density EEG (hdEEG) data collected during resting state on 19 healthy subjects. We calculated EEG connectivity maps for each main DMN node, and for different brain rhythms. We then focused on pairs of DMN nodes, and conducted an analysis of frequency-dependent connectivity profiles. This permitted us to test the existence of shared and connection-specific intrinsic interactions in the DMN.

2. Materials and methods

2.1. EEG data acquisition

Eyes-open resting state EEG data were collected in 19 healthy young adult volunteers (age 28 ± 6 years, 14 females). Ethical approval was granted by the Ethics Committee of ETH Zurich. The experiment was performed in accordance with the relevant guidelines and regulations, and informed consent was obtained from all participants. For each volunteer, we recorded EEG signals at 1000Hz sampling rate using a 256-channel HydroCel Geodesic Sensor Net by Electrical Geodesics (Eugene, Oregon, USA). The eyes open condition, which lasted 5 min, was used to ensure that the participant would maintain wakefulness during EEG data acquisition (Tagliazucchi and Laufs, 2014). Positions of EEG sensors as well as of three landmarks (nasion, left and right preauricolar) were localized in the same experimental session using a Geodesic Photogrammetry System (Russell et al., 2005). Moreover, we acquired a T1-weighted whole-head anatomical image in a separate experimental session, using a Philips Ingenia 3T Magnetic Resonance (MR) scanner (Best, The Nederlands). To this end, we used a turbo field echo sequence with the following scanning parameters: TR = 8.25 ms, TE = 3.8 ms, flip angle = 8°, voxel size: 1 mm^3 isotropic.

2.2. fMRI data acquisition

Eyes-open resting state fMRI data were collected in 24 healthy volunteers (20-31 years old, 15 females). These data have been already used in previous studies (Liu et al., 2018; Mantini et al., 2012; Mantini and Vanduffel, 2013). Ethical approval was granted by the Ethics Committee of Creighton University. The experiment was performed in accordance with the relevant guidelines and regulations, and informed consent was obtained from all participants. The functional images were obtained using a Philips Achieva 3T MR scanner. More specifically, T2*-weighted echo-planar imaging (EPI) with blood oxygen level dependent (BOLD) contrast was used. The scanning parameters were the following: 32 axial slices, 230 × 230 in-plane matrix, TR/TE = 2000/35, flip angle = 90°, voxel size = 2.875 × 2.875 × 3.5 mm^3, 300 dynamic volumes. Furthermore, a 3D high-resolution T1-weighted image, to be used for anatomical reference, was collected by means of an MP-RAGE sequence. The scanning parameters were: TR = 9.1 ms, TE = 3.7 ms, flip angle = 8°, voxel size = 0.938 × 0.938 × 1 mm^3.

2.3. fMRI preprocessing and connectivity analysis

FMRI data were preprocessed using standard procedures for functional connectivity analyses, including head motion correction, registration to brain anatomy, band-pass filtering (0.01–0.1 Hz), regression of white matter, cerebrospinal fluid and global signals, and spatial smoothing at 6 mm full width half maximum (Gavrilescu et al., 2008). Regions of interest (ROIs) were selected using the DMN spatial map reported in (Liu et al., 2017). Specifically, we defined MNI coordinates for the following four brain regions, which are those more consistently

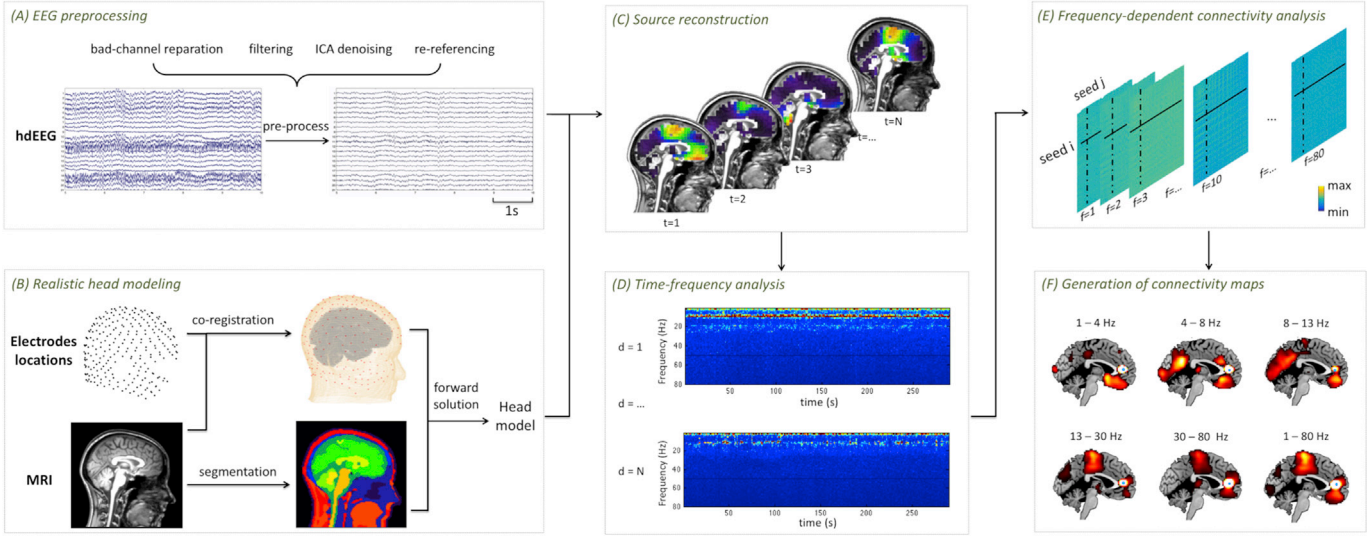

Fig. 1. Seed-based connectivity analysis workflow for hdEEG recordings. (A) EEG preprocessing, including bad-channel repair, filtering, artifact removal and re-referencing; (B) Realistic head model creation, involving electrodes co-registration, MRI segmentation and forward model solution; (C) Reconstruction of neural source dynamics by source localization; (D) Time-frequency analysis of neuronal activity in each voxel; (E) Calculation of frequency-dependent connectivity; (F) Generation of single-subject connectivity maps for specific frequency bands (e.g. delta (1-4 Hz), theta (4-8 Hz), alpha (8-13 Hz), beta (13-30 Hz), gamma (30-80 Hz) and fullband (1-80 Hz)).

reported in the literature as belonging to the DMN (Buckner et al., 2008; Mantini and Vanduffel, 2013): MPFC, PCC, LANG and RANG (Table S1). By inverting the spatial transformation required to register the individual MR image to MNI space, the ROI coordinates in individual MR space could be identified. The ROIs were spherical, centered over its coordinates in individual MR space, and with 6 mm radius. We applied principal component analysis (PCA) on the timecourses from all voxels included in the spherical ROI. The first principal component was considered as representative of the activity in the whole ROI, rather than the average of its voxel timecourses, aiming at the reduction of spatial leakage effects (Chang et al., 2015; Gao et al., 2013). FMRI connectivity maps were calculated by correlating the fMRI time-course of the seed ROI with the timecourses of all the voxels in the gray matter. These maps were generated in native MR space, and then non-linearly registered to MNI space to facilitate across-subject comparisons. Group-level connectivity maps were obtained by calculating a one-sample *t*-test across individual maps. The significance level was corrected for multiple comparisons using the false discovery rate (FDR) approach (Benjamini and Hochberg, 1995).

2.4. EEG preprocessing and source reconstruction

We used the same automated analysis workflow as in (Liu et al., 2017) to estimate source-space neural data from the EEG recordings (Fig. 1). *EEG preprocessing* (Fig. 1A). First, the channels with poor signal quality were identified by calculating the Pearson correlation, in a chosen frequency band, between their signal and the signal from all the other channels, or according to their noise variance, estimated in a frequency range where the contribution of the brain activity can be considered negligible (from 200 to 250 Hz). These bad channels (from 0 to 13, depending on the dataset) were corrected by interpolating the respective timecourses from the neighboring channels. After, the data were band-pass filtered in the frequency band 1–80Hz and the biological artefacts were rejected using the Indipendent Component Analysis (ICA). Indipendent Components (ICs) were estimated with a fast fixed-point ICA (FastICA) algorithm based on a deflation approach and hyperbolic tangent as contrast function (Mantini et al., 2008). A classification of the ICs was done according to three parameters: 1) correlation with the power of the Electrooculografic (EOG) and Electromyografic (EMG) signals, simultaneously acquired with the EEG recordings; 2) similarity of the spectrum with the $1/f$ function; 3) kurtosis values. The timecourses of the ICs classified as bad were reconstructed at the channel level and then subtracted from the data. Finally, the EEG signals were re-referenced with an optimized version of the Reference Electrode Standardization Technique (REST) (Liu et al., 2015; Mantini et al., 2008; Yao, 2001; Yao et al., 2005). *Realistic head modeling* (Fig. 1B). The anatomical MR image was segmented in 12 different compartments: skin, eyes, muscle, fat, spongy bone, compact bone, cortical gray matter, cerebellar gray matter, cortical white matter, cerebellar white matter, cerebrospinal fluid and brain stem. Then, the EEG sensors were rigidly co-registered to the head contour (outer layer of the skin compartment) with a three-steps procedure including: projection of the electrode coordinates in the individual space through a rigid-body transformation, estimated on the positions of the anatomical landmarks; alignment of the electrode positions to the head contour using the Iterative Closest Point registration algorithm; projection of each electrode onto the surface point with the smallest Euclidean distance. Conductivity values for each head compartment were set based on previous literature (Haueisen et al., 1997). Dipole sources were constrained by a regular 6 mm grid spanning both the cortical/subcortical and the cerebellar gray matter. Then, a realistic head model was generated by using SimBio (https://www.mrt.uni-jena.de/simbio), a whole-head finite element model (Wolters et al., 2004). *Source reconstruction* (Fig. 1C). The realistic head model was provided as input to the exact low-resolution brain electromagnetic tomography (eLORETA) algorithm (Pascual-Marqui et al., 2011), together with the preprocessed EEG signals, to estimate brain activity in the source space at high-temporal resolution.

2.5. EEG connectivity maps for distinct brain rhythms

After reconstructing source-space activity in the gray matter, we performed, for each timecourse, a time-frequency decomposition with the short-time Fourier transform (Fig. 1D). Specifically, we used a Hamming window of 2 s, with 50% overlap between consecutive windows, to reconstruct frequencies in the range 1–80Hz, at steps of 1Hz. The same ROIs used for fMRI connectivity analysis (Table S1) were defined in the individual EEG source space. EEG connectivity maps were created by estimating the statistical dependence between the power time-course of the seed ROI and the power time-courses of gray matter voxels. For each seed-voxel pair, we removed, frequency-by-frequency, the contribution of coherent zero-lag activity from the two time-courses (Hipp et al., 2012). Then, we applied a logarithmic transformation to the signal-orthogonalized power time-courses, calculated the Pearson correlation between them, and derived z-values by using the r-to-z Fisher's transform (Fig. 1E). The connectivity map for a given brain rhythm was obtained by averaging the z-value connectivity maps

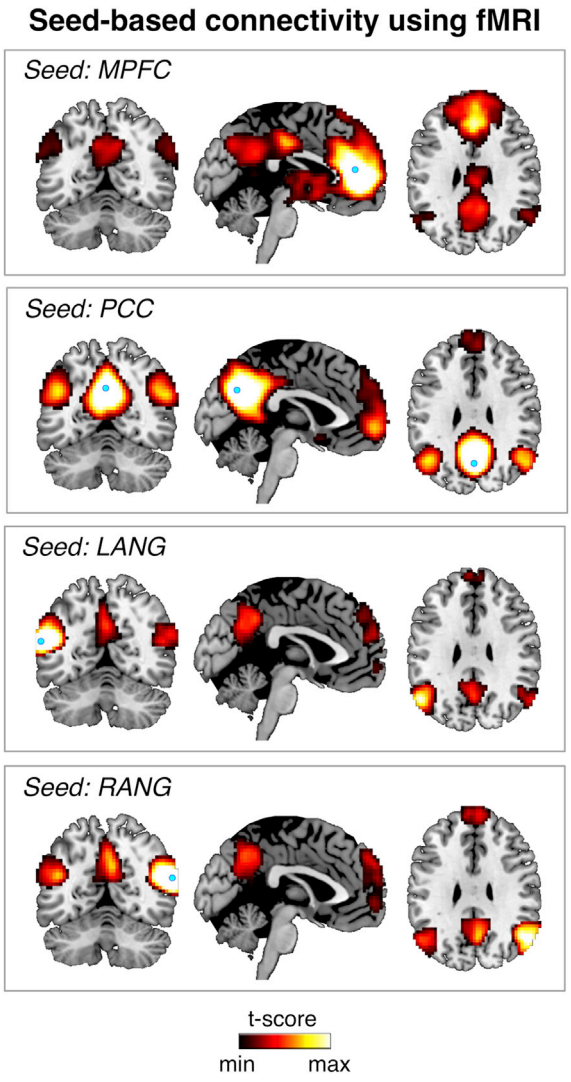

Fig. 2. fMRI connectivity maps for DMN. These maps were compared with the hdEEG connectivity maps obtained from the same seed regions (light blue dot): MPFC, PCC, LANG, and RANG. Spatial maps are shown in coronal, sagittal and axial sections. The significance level is set to $p < 0.01$, FDR corrected.

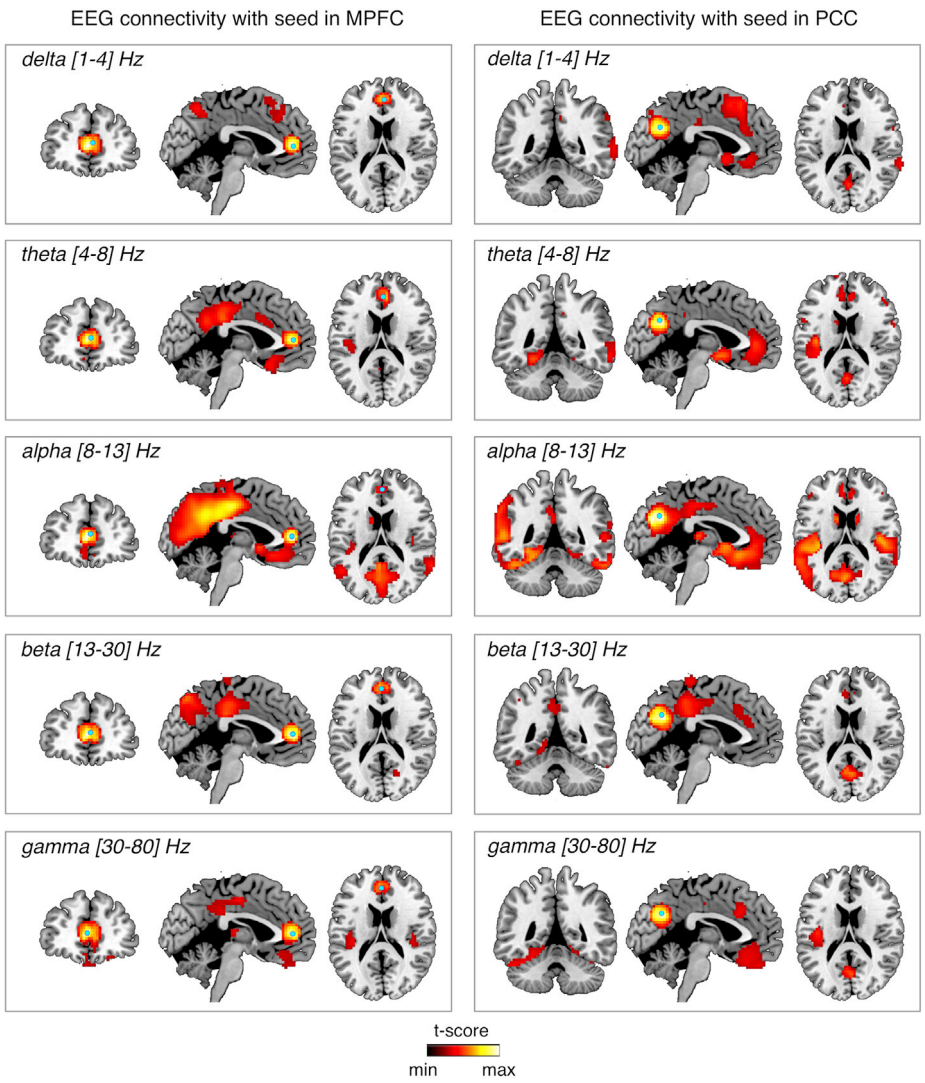

Fig. 3. hdEEG connectivity maps for different frequency bands. Connectivity was calculated for MPFC and PCC as seed regions (light blue dot), respectively, in delta (1-4 Hz), theta (4-8 Hz), alpha (8-13 Hz), beta (13-30 Hz), and gamma (30-80 Hz) bands. Spatial maps are shown in coronal, sagittal and axial sections. The significance level is set to $p < 0.05$, FDR corrected.

calculated for each individual frequency within the relevant range (delta, 1-4 Hz; theta, 4-8 Hz; alpha, 8-13 Hz; beta, 13-30 Hz; gamma, 30-80 Hz; full-band, 1-80 Hz) (Fig. 1F). To assess the statistical significance of the connectivity results across participants, we performed a one-sample one-sided *t*-test, separately for each frequency band. Then, we corrected the significance level for multiple comparisons using the FDR procedure (Benjamini and Hochberg, 1995).

2.6. Correspondence between EEG and fMRI connectivity maps

We compared the spatial pattern of the EEG connectivity maps for specific frequency bands with the one of fMRI connectivity maps, obtained considering the same seed. To quantify the spatial correspondence between EEG and fMRI connectivity maps at the group level, we used the Spearman correlation. This is a nonparametric measure of correlation, ranging between −1 and 1. It is equal to ±1 when there is a perfect monotonic relationship between values in corresponding maps, and equal to 0 when there is no clear tendency (Wayne, 1990).

2.7. Analysis of frequency-dependent EEG connectivity

Besides the analysis of EEG connectivity maps, we also examined the profile of EEG connectivity for specific pairs of ROIs, frequency-by-frequency (Fig. 1E). The significance of the frequency-dependent connectivity profiles across individuals was assessed by using a one-sample *t*-test, in combination with FDR to account for multiple comparisons. After setting the significance level at $p < 0.01$ FDR corrected, we examined the global pattern of ROI-to-ROI connectivity at each frequency. Specifically, we evaluated if there were frequencies for which there was connectivity between each DMN node pair (shared intrinsic interaction) or between single pairs only (connection-specific intrinsic interaction).

3. Results

To validate the positions of the selected DMN nodes, namely PCC, MPFC, LANG and RANG, we calculated seed-based connectivity maps from resting-state fMRI data. Group-level fMRI maps showed a spatial distribution largely resembling the DMN for all the chosen seeds (Fig. 2). These DMN regions were then used to study the functional interactions between those nodes in relation to different brain rhythms. To this end, we used hdEEG data and calculated connectivity maps for frequency bands associated with delta, theta, alpha, beta and gamma rhythms, respectively (Fig. 3 and Fig. S1). The importance of the frequency band considered for studying the connectivity pattern was overt when comparing the group-level fMRI maps with the corresponding EEG maps. For any of the four seed regions, the largest spatial similarity with the

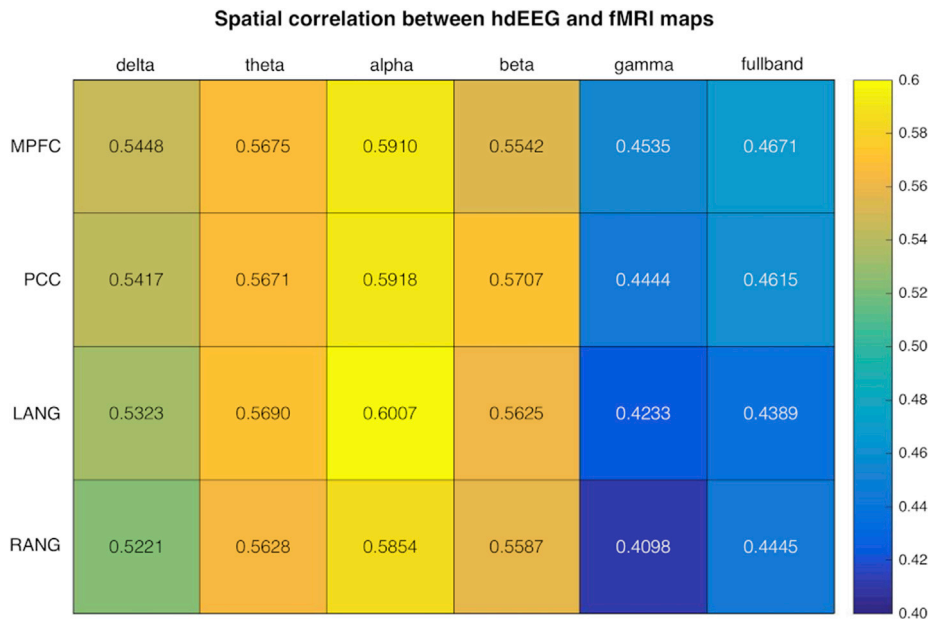

Fig. 4. Spatial correlation between hdEEG and fMRI connectivity maps from corresponding DMN seeds. Single-subject EEG connectivity maps were obtained for delta, theta, alpha, beta, gamma bands, and fullband and, then, compared to the corresponding fMRI maps averaged across subjects.

DMN pattern reconstructed from fMRI data was obtained for hdEEG maps in the alpha frequency range (Fig. 3 and Fig. S1). Spatial correlation values between fMRI and EEG maps for any specific frequency band were larger than those obtained using full-band (1-80 Hz) EEG power. We found relatively high correlations also for the theta and beta frequency bands, and relatively lower values for the gamma band (Fig. 4).

We then examined the frequency profile of the connectivity between pairs of DMN areas to identify the specific frequencies supporting functional interactions across the whole network. Our data showed that the DMN nodes were all connected to each other in the high theta and alpha bands ($p < 0.001$), peaking at 9-11 Hz. For each pair of seeds, connectivity was significant ($p < 0.01$) in correspondence of distinct sets of frequencies in the beta and gamma bands (Fig. 5). Interestingly, the connectivity between MPFC and the other three nodes reached the significance level in the gamma band (Fig. 6A, red, orange and yellow bars), as well as in the beta band between PCC and the bilateral ANGs (Fig. 6A, green and light blue bars). This frequency-specificity emerged also when examining functional connectivity maps at specific frequencies. For instance, the PCC was found to be connected at 10 Hz with MPFC, LANG and RANG, as expected based on previous analyses (Figs. 3-5). On the other hand, PCC selectively interacted with MPFC, and not with LANG/RANG, at 14 Hz. Conversely, interactions were strong between PCC and LANG/RANG at 17 Hz, whereas they were less prominent between PCC and MPFC at the same frequency (Fig. 6B).

4. Discussion

In this study, we have investigated neuronal oscillations supporting intrinsic interactions within the DMN. To this end we have employed an advanced approach to estimate frequency-dependent functional interactions using hdEEG data. Our results suggested that a remarkable spatial similarity with fMRI connectivity patterns can be obtained when EEG connectivity is assessed in the alpha frequency range (Figs. 3-4 and Fig. S1). More in general, we found the spatial similarity with fMRI connectivity maps to be largely dependent on the frequency band considered for EEG data analysis (Fig. 4). Notably, EEG connectivity patterns were related not only to the frequency band considered, but - to a large extent - depended also on the node selected as seed (Fig. 3 and Fig. S1). Our data showed that each pair of DMN nodes peaked at about the same frequency in the alpha range, but also showed significant connectivity at specific frequencies in the beta and gamma bands (Figs. 5-6). Overall, the similarity between connectivity profiles reported for different DMN connections in the alpha band and the spatial specificity that emerges when reconstructing connectivity maps in a narrower frequency interval support the idea that the exchange of information among the nodes of the network is achieved through both shared and connection-specific neuronal oscillations. We will further elaborate on the points above in the following paragraphs.

4.1. Topology of band-limited DMN connectivity maps

The DMN connectivity maps were highly dependent both on the seed region, and on the frequency band considered. For each node, we compared the fMRI connectivity maps (Fig. 2) with the corresponding ones from EEG source-reconstructed data in delta (1-4 Hz), theta (4-8 Hz), alpha (8-13 Hz), beta (13-30 Hz), and gamma (30-80 Hz) bands (Fig. 3 and Fig. S1). The complete pattern was reconstructed only when considering alpha oscillations, regardless of the chosen seed (Figs. 4-5). This suggests that the alpha rhythm is used for the exchange of information across the whole DMN (Brookes et al., 2011; de Pasquale et al., 2010; Hipp et al., 2012; Mantini et al., 2007; Marino et al., 2019; Tang et al., 2017; Zhang et al., 2018). Based on the connectivity maps derived for different brain rhythms, we posit that the beta and gamma oscillations might support selective communication within DMN sub-networks (Fig. 3 and Fig. S1). As gamma band activity in EEG recordings commonly presents small intensities, and can be easily masked by noise, findings in this frequency band might just derive from spurious correlations. Nonetheless, the spatial specificity of the connectivity maps obtained for the gamma rhythm (Fig. 3 and Fig. S1) suggests that the observed results are not caused by artifacts, but, on the contrary, are expression of genuine neuronal activity. Computational modelling may permit to elucidate to what extent and under what conditions gamma band signals carry complementary information to alpha and beta oscillations, reflecting functionally-distinct processes of neuronal communication (Buzsáki and Wang, 2012). Further work should be conducted to examine not only the connectivity strength, but also the direction of the information flow between brain regions (Hillebrand et al., 2016), at different frequencies and spatial scales.

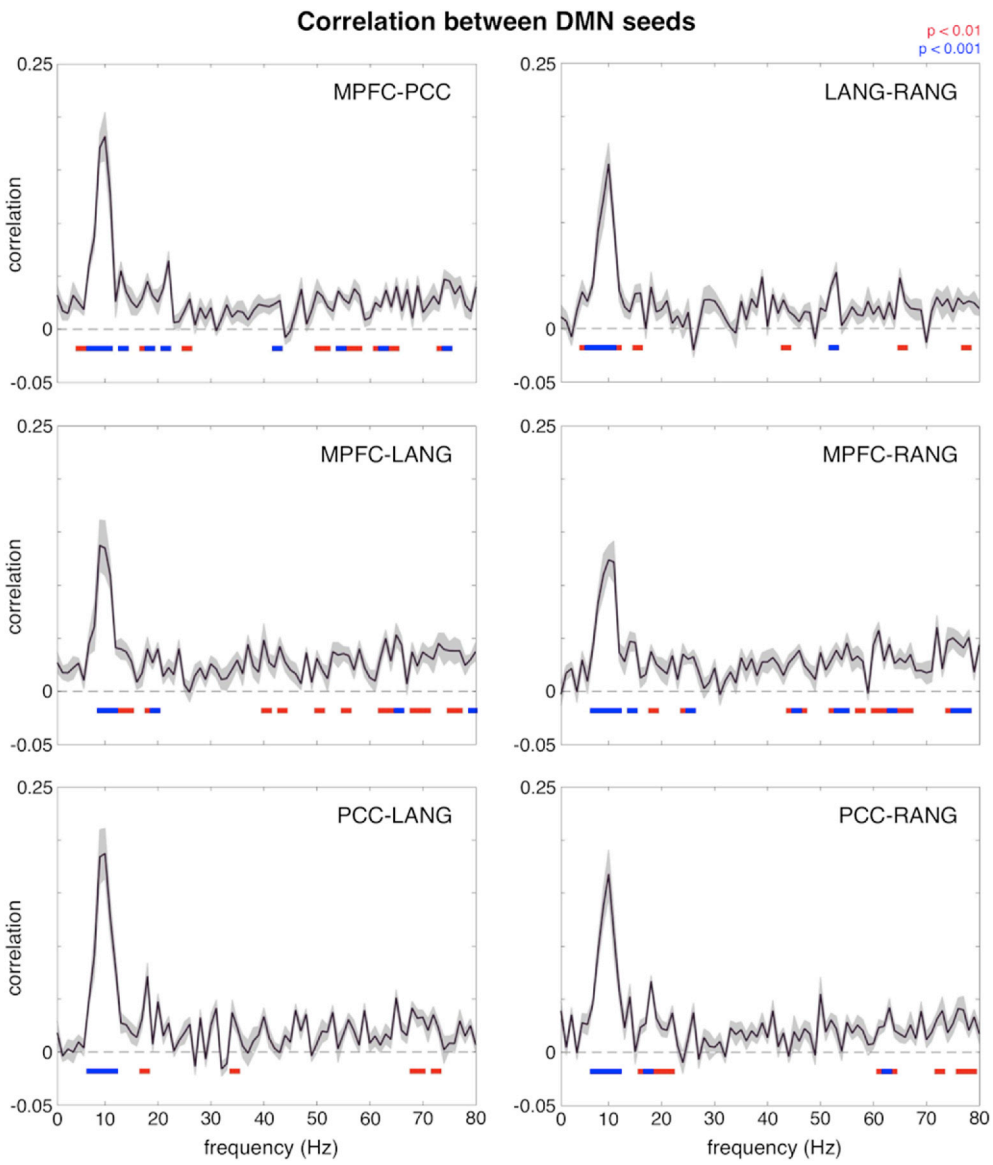

Fig. 5. Frequency-dependent connectivity between pairs of DMN regions. Frequency-dependent connectivity profiles for the six possible connections between pairs of DMN seeds: MPFC-PCC, LANG-RANG, MPFC-LANG, MPFC-RANG, PCC-LANG, PCC-RANG. The lines at the bottom of each panel indicate the frequency range where the connectivity is significantly above the average in the whole brain (one-sample *t*-test, FDR corrected $p < 0.01$ and $p < 0.001$ indicated with a red and a blue bar, respectively).

4.2. *Frequency-dependent functional interactions within the DMN*

Previous MEG studies employed a seed-based approach to investigate frequency-dependent connectivity in a restricted number of task-related brain networks (Hipp et al., 2012), and, more recently, in two regions of the DMN (Tang et al., 2017). To the best of our knowledge, this is the first study that examined what neuronal oscillations underlie the interactions between several DMN nodes. Our connectivity results (Fig. 6A) confirm the idea that the PCC is a DMN hub, possibly mediating information exchange and integration across different brain regions (Fransson and Marrelec, 2008; Leech et al., 2012). They also suggested that a common carrier frequency at 9-11 Hz may allow the exchange of information across DMN nodes (Brookes et al., 2011; de Pasquale et al., 2010; Hipp et al., 2012; Tang et al., 2017), and other frequencies may be selectively engaged when the interaction involves only part of the network (Figs. 5-6). Notably, we found evidence that long-range communication might occur in the alpha band, whereas short-range interactions might take place at higher frequencies (i.e. PCC-LANG and PCC-RANG connectivity in beta and gamma bands). This is consistent with previous studies suggesting that short- and long-range connectivity are mediated by higher and lower frequencies, respectively (Canolty et al., 2006; Deco et al., 2009; Ganzetti and Mantini, 2013; Hacker et al., 2017; Jones et al., 2000; Kopell et al., 2000; Lopes da Silva, 2013). Taken together, our findings suggest that amplitude modulation at specific frequencies is a possible mechanism used to facilitate communication between two brain areas (Akam and Kullmann, 2014, 2010).

4.3. *Study limitations*

A number of limitations of this study should be considered. First, we could not compare EEG- and fMRI-based connectivity maps at the individual level as the cohorts of participants for the fMRI and EEG acquisitions were not the same. Analyses of EEG- and fMRI-based connectivity maps at the individual level may lead to a better understanding of the similarities in the results obtained using different imaging modalities. Second, this similarity was quantified using canonical correlations. We believe this comparison is informative, as it can highlight which frequency band yields the best correspondence between EEG- and fMRI-based connectivity. However, the canonical correlation analysis does not take into account possible interactions between different frequency bands. As such, multivariate approaches, including partial correlation analyses, may be used in future studies to examine in more detail EEG-fMRI correspondences. Finally, the seed regions used in the present study included the four main DMN nodes. In line of principle, it would be

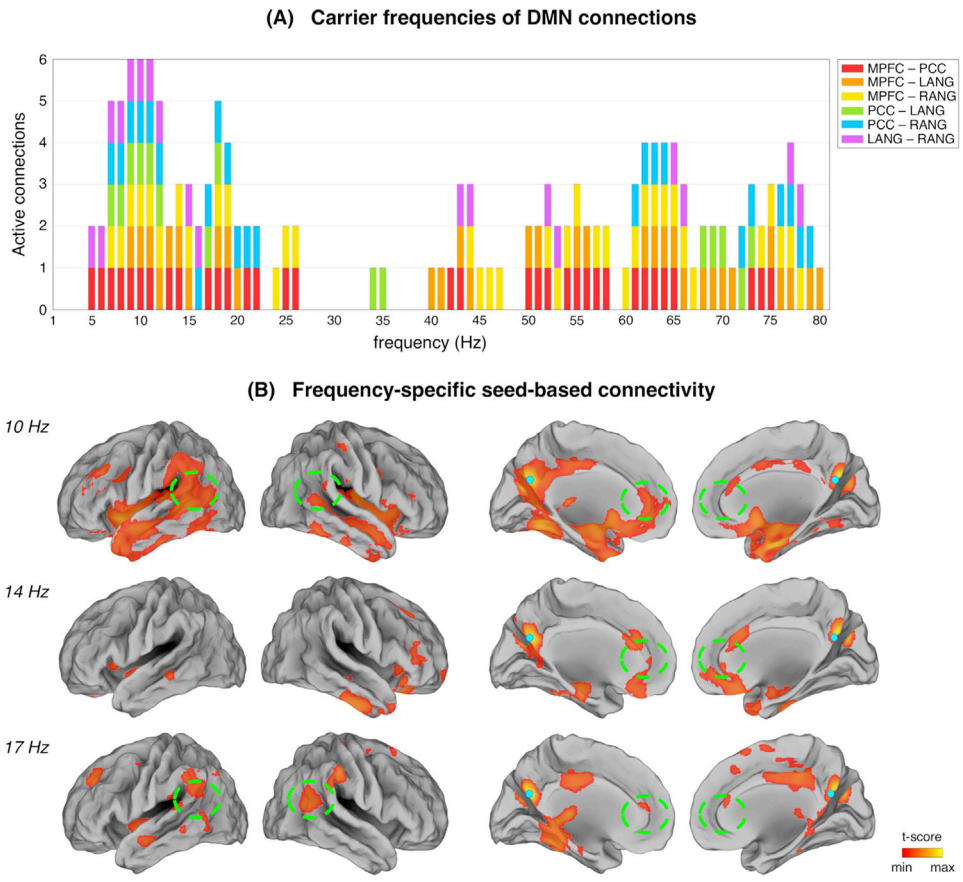

Fig. 6. Frequency specificity in DMN connections. (A) Carrier frequencies for each connection between DMN seed regions. The significance level is set to $p < 0.01$, FDR-corrected. (B) Qualitative visualization of the functional connections of the PCC (light blue dot) at three different frequencies: at 10 Hz all the nodes (dashed green circles) are connected with each other, thus also with the seed, as expected from the statistical analysis presented in Fig. 6A where for the same frequency the connections PCC-MPFC (red bar), PCC-LANG (green bar) and PCC-RANG (blue bar) are all significant; at 14 Hz PCC is connected only with MPFC, therefore neither LANG nor RANG are visible in the corresponding map; at 17Hz its connections with bilateral ANGs are significant, as well as PCC-MPFC.

possible to investigate the EEG connectivity pattern for other seed regions putatively belonging to the DMN. On the other hand, it should be considered that the selected seed regions should not be too close to each other. The spatial precision that can be achieved with EEG is potentially lower than with other brain imaging modalities. In particular, connectivity analyses based on EEG data suffer from the spatial leakage problem (Liu et al., 2017; Siems et al., 2016), which imposes a limit to the minimum distance between two brain regions in order to obtain a meaningful and reliable estimate of their connectivity. Another caveat of the present study concerns temporal rather than spatial aspects associated with the chosen connectivity measure. In particular, it should be noted that connectivity was quantified through correlations of band-limited power, which was obtained using a window with specific length. Future studies are warranted to examine the effect of different window lengths, and should in particular aim to investigate the non-stationarity of EEG connectivity measures (de Pasquale et al., 2010; Yuan et al., 2016).

5. Conclusion and future perspectives

By examining intrinsic functional interactions emerging from hdEEG data, we have provided new insight into the role of neuronal oscillations in shaping the DMN. Importantly, our approach for connectivity analysis of hdEEG data can be applied in future studies to probe not only intra- but also inter-network connectivity patterns (de Pasquale et al., 2012). Also, in the current study we focused on the analysis of large-scale functional interactions in the resting state, but it would also be interesting to examine how frequency-dependent connectivity is modulated by task performance (Watrous et al., 2013), or different levels of consciousness during sleep (Buzsaki et al., 2004). Another avenue for future research is the investigation of the variability in EEG connectivity measures across participants, as for instance in the context of aging studies (Babaeeghazvini et al., 2019). Last but not least, the use of EEG connectivity measures in clinical studies may be promising, in particular for brain disorders in which synaptic transmission is altered, such as in autism and schizophrenia (Bourgeron, 2009; Uhlhaas and Singer, 2010, 2006), and long-range neuronal synchronization is therefore put forward as a potential clinical marker.

Acknowledgements

The work was supported by the KU Leuven Special Research Fund, Belgium (grant C16/15/070), the Research Foundation Flanders (grants G0F76.16N, G0936.16N, EOS.30446199 and fellowship 12P6719N to QL) and the James G. Boswell Foundation (postdoctoral fellowship to QL).

Appendix A. Supplementary data

Supplementary data to this article can be found online at https://doi.org/10.1016/j.neuroimage.2019.07.007.

References

Akam, T., Kullmann, D.M., 2014. Oscillatory multiplexing of population codes for selective communication in the mammalian brain. Nat. Rev. Neurosci. 15, 111–122. https://doi.org/10.1038/nrn3668.

Akam, T., Kullmann, D.M., 2010. Oscillations and filtering networks support flexible routing of information. Neuron 67, 308–320. https://doi.org/10.1016/j.neuron.2010.06.019.

Andrews-hanna, J.R., Reidler, J.S., Sepulcre, J., Poulin, R., Buckner, R.L., 2010. Functional-anatomic fractionation of the brain's default network. Neuron 65, 550–562. https://doi.org/10.1016/j.neuron.2010.02.005.Functional-Anatomic.

Assaf, M., Jagannathan, K., Calhoun, V.D., Miller, L., Stevens, M.C., Sahl, R., O'Boyle, J.G., Schultz, R.T., Pearlson, G.D., 2010. Abnormal functional connectivity of default mode sub-networks in autism spectrum disorder patients. Neuroimage 53, 247–256. https://doi.org/10.1016/j.neuroimage.2010.05.067.

Babaeeghazvini, P., Rueda-Delgado, L.M., Zivari Adab, H., Gooijers, J., Swinnen, S., Daffertshofer, A., 2019. A combined diffusion-weighted and electroencephalography

study on age-related differences in connectivity in the motor network during bimanual performance. Hum. Brain Mapp. 40, 1799–1813. https://doi.org/10.1002/hbm.24491.
Benjamini, Y., Hochberg, Y., 1995. Controlling the False Discovery Rate: a practical and powerful approach to multiple testing. J. R. Stat. Soc. 57, 289–300.
Bourgeron, T., 2009. A synaptic trek to autism. Curr. Opin. Neurobiol. 19, 231–234. https://doi.org/10.1016/j.conb.2009.06.003.
Brookes, M.J., Woolrich, M., Luckhoo, H., Price, D., Hale, J.R., Stephenson, M.C., Barnes, G.R., Smith, S.M., Morris, P.G., 2011. Investigating the electrophysiological basis of resting state networks using magnetoencephalography. Proc. Natl. Acad. Sci. 108, 16783–16788. https://doi.org/10.1073/pnas.1112685108.
Buckner, R.L., Andrews-Hanna, J.R., Schacter, D.L., 2008. The brain's default network: anatomy, function, and relevance to disease. Ann. N. Y. Acad. Sci. 1124, 1–38. https://doi.org/10.1196/annals.1440.011.
Buckner, R.L., Carroll, D.C., 2007. Self-projection and the brain. Trends Cognit. Sci. https://doi.org/10.1016/j.tics.2006.11.004.
Buzsaki, G., Draughn, A., Buzsáki, G., Draguhn, A., Buzsaki, G., Draughn, A., 2004. Neuronal oscillations in cortical networks. Science 304, 1926–1930. https://doi.org/10.1126/science.1099745.
Buzsáki, G., Wang, X.-J., 2012. Mechanisms of gamma oscillations. Annu. Rev. Neurosci. 35, 203–225. https://doi.org/10.1146/annurev-neuro-062111-150444.Mechanisms.
Canolty, R.T., Edwards, E., Dalal, S.S., Soltani, M., Nagarajan, S.S., Berger, M.S., Barbaro, N.M., Knight, R.T., 2006. High gamma power is phase-locked to theta oscillations in human neocortex. Science 313, 1626–1628, 80. https://doi.org/10.1126/science.1128115.High.
Chang, W.-T., Jääskeläinen, I.P., Belliveau, J.W., Huang, S., Hung, A.-Y., Rossi, S., Ahveninen, J., 2015. Combined MEG and EEG show reliable patterns of electromagnetic brain activity during natural viewing. Neuroimage 114, 49–56. https://doi.org/10.1109/EMBC.2016.7590696.Upper.
Chen, J.E., Glover, G.H., Greicius, M.D., Chang, C., 2017. Dissociated patterns of anti-correlations with dorsal and ventral default-mode networks at rest. Hum. Brain Mapp. 38, 2454–2465. https://doi.org/10.1002/hbm.23532.
de Pasquale, F., Della Penna, S., Snyder, A.Z., Lewis, C., Mantini, D., Marzetti, L., Belardinelli, P., Ciancetta, L., Pizzella, V., Romani, G.L., Corbetta, M., 2010. Temporal dynamics of spontaneous MEG activity in brain networks. Proc. Natl. Acad. Sci. 107, 6040–6045. https://doi.org/10.1073/pnas.0913863107.
de Pasquale, F., Penna, S. Della, Snyder, A.Z., Marzetti, L., Pizzella, V., Romani, G.L., Corbetta, M., 2012. A cortical core for dynamic integration of functional networks in the resting human brain. Neuron 74, 753–764. https://doi.org/10.1038/nature13314.A.
Deco, G., Jirsa, V., McIntosh, A.R., Sporns, O., Kotter, R., 2009. Key role of coupling, delay, and noise in resting brain fluctuations. Proc. Natl. Acad. Sci. 106, 10302–10307. https://doi.org/10.1073/pnas.0901831106.
Fransson, P., Marrelec, G., 2008. The precuneus/posterior cingulate cortex plays a pivotal role in the default mode network: evidence from a partial correlation network analysis. Neuroimage 42, 1178–1184. https://doi.org/10.1016/j.neuroimage.2008.05.059.
Ganzetti, M., Mantini, D., 2013. Functional connectivity and oscillatory neuronal activity in the resting human brain. Neuroscience 240, 297–309. https://doi.org/10.1016/j.neuroscience.2013.02.032.
Gao, L., Zhang, T., Wang, J., Stephen, J., 2013. Facilitating neuronal connectivity analysis of evoked responses by exposing local activity with principal component analysis preprocessing: simulation of evoked MEG. Brain Topogr. 26, 201–211 (Investigations). https://doi.org/10.1016/j.pestbp.2011.02.012.
Gavrilescu, M., Stuart, G.W., Rossell, S., Henshall, K., McKay, C., Sergejew, A.A., Copolov, D., Egan, G.F., 2008. Functional connectivity estimation in fMRI data: influence of preprocessing and time course selection. Hum. Brain Mapp. 29, 1040–1052. https://doi.org/10.1002/hbm.20446.
Greicius, M.D., Krasnow, B., Reiss, A.L., Menon, V., 2003. Functional connectivity in the resting brain: a network analysis of the default mode hypothesis. Proc. Natl. Acad. Sci. U.S.A. 100, 253–258. https://doi.org/10.1073/pnas.0135058100.
Hacker, C.D., Snyder, A.Z., Pahwa, M., Corbetta, M., Leuthardt, E.C., 2017. Frequency-specific electrophysiologic correlates of resting state fMRI networks. Neuroimage 149, 446–457. https://doi.org/10.1177/0003122413519445.Are.
Haueisen, J., Ramon, C., Eiselt, M., Brauer, H., Nowak, H., 1997. Influence of tissue resistivities on neuromagnetic fields and electric potentials studied with a finite element model of the head. IEEE Trans. Biomed. Eng. 44, 727–735. https://doi.org/10.1109/10.605429.
Hillebrand, A., Tewarie, P., van Dellen, E., Yu, M., Carbo, E.W.S., Douw, L., Gouw, A.A., van Straaten, E.C.W., Stam, C.J., 2016. Direction of information flow in large-scale resting-state networks is frequency-dependent. Proc. Natl. Acad. Sci. 113, 3867–3872. https://doi.org/10.1073/pnas.1515657113.
Hipp, J.F., Hawellek, D.J., Corbetta, M., Siegel, M., Engel, A.K., 2012. Large-scale cortical correlation structure of spontaneous oscillatory activity. Nat. Neurosci. 15, 884–890. https://doi.org/10.1038/nn.3101.Large-scale.
Hyatt, C.J., Calhoun, V.D., Pearlson, G.D., Assaf, M., 2015. Specific default mode subnetworks support mentalizing as revealed through opposing network recruitment by social and semantic FMRI tasks. Hum. Brain Mapp. 36, 3047–3063. https://doi.org/10.1002/hbm.22827.
Jones, S.R., Pinto, D.J., Kaper, T.J., Kopell, N., 2000. Alpha-frequency rhythms desynchronize over long cortical distances: a modeling study. J. Comput. Neurosci. 9, 271–291. https://doi.org/10.1023/A:1026539805445.
Kopell, N., Ermentrout, G.B., Whittington, M.A., Traub, R.D., 2000. Gamma rhythms and beta rhythms have different synchronization properties. Proc. Natl. Acad. Sci. 97, 1867–1872. https://doi.org/10.1073/pnas.97.4.1867.
Leech, R., Braga, R., Sharp, D.J., 2012. Echoes of the brain within the posterior cingulate cortex. J. Neurosci. 32, 215–222. https://doi.org/10.1523/JNEUROSCI.3689-11.2012.
Liu, Q., Balsters, J.H., Baechinger, M., Van Der Groen, O., Wenderoth, N., Mantini, D., 2015. Estimating a neutral reference for electroencephalographic recordings: the importance of using a high-density montage and a realistic head model. J. Neural Eng. 12, 56012. https://doi.org/10.1088/1741-2560/12/5/056012.
Liu, Q., Farahibozorg, S., Porcaro, C., Wenderoth, N., Mantini, D., 2017. Detecting large-scale networks in the human brain using high-density electroencephalography. Hum. Brain Mapp. 38, 4631–4643. https://doi.org/10.1002/hbm.23688.
Liu, Q., Ganzetti, M., Wenderoth, N., Mantini, D., 2018. Detecting large-scale brain networks using EEG: impact of electrode density, head modeling and source localization. Front. Neuroinf. 12, 1–11. https://doi.org/10.3389/fninf.2018.00004.
Lopes da Silva, F., 2013. EEG and MEG: relevance to neuroscience. Neuron 80, 1112–1128. https://doi.org/10.1016/j.neuron.2013.10.017.
Mantini, D., Franciotti, R., Romani, G.L., Pizzella, V., 2008. Improving MEG source localizations: an automated method for complete artifact removal based on independent component analysis. Neuroimage 40, 160–173. https://doi.org/10.1016/j.neuroimage.2007.11.022.
Mantini, D., Hasson, U., Betti, V., Perrucci, M.G., Romani, G.L., Corbetta, M., Orban, G.A., Vanduffel, W., 2012. Inter-species activity correlations reveal functional correspondences between monkey and human brain areas. Nat. Methods 9, 277–282. https://doi.org/10.1117/12.2008529.Image-based.
Mantini, D., Perrucci, M.G., Del Gratta, C., Romani, G.L., Corbetta, M., 2007. Electrophysiological signatures of resting state networks in the human brain. Proc. Natl. Acad. Sci. U.S.A. 104, 13170–13175. https://doi.org/10.1073/pnas.0700668104.
Mantini, D., Vanduffel, W., 2013. Emerging roles of the brain's default network. Neuroscientist 19, 76–87. https://doi.org/10.1177/1073858412446202.
Marino, M., Liu, Q., Samogin, J., Tecchio, F., Cottone, C., Mantini, D., Porcaro, C., 2019. Neuronal dynamics enable the functional differentiation of resting state networks in the human brain. Human brain mapping 40 (5), 1445–1457. https://doi.org/10.1002/hbm.24458.
Pascual-Marqui, R.D., Lehmann, D., Koukkou, M., Kochi, K., Anderer, P., Saletu, B., Tanaka, H., Hirata, K., John, E.R., Prichep, L., Biscay-Lirio, R., Kinoshita, T., 2011. Assessing interactions in the brain with exact low-resolution electromagnetic tomography. Philos. Trans. R. Soc. A Math. Phys. Eng. Sci. 369, 3768–3784. https://doi.org/10.1098/rsta.2011.0081.
Raichle, M.E., MacLeod, A.M., Snyder, A.Z., Powers, W.J., Gusnard, D.A., Shulman, G.L., 2001. A default mode of brain function. Proc. Natl. Acad. Sci. U.S.A. 98, 676–682. https://doi.org/10.1073/pnas.98.2.676.
Russell, G.S., Eriksen, K.J., Poolman, P., Luu, P., Tucker, D.M., 2005. Geodesic photogrammetry for localizing sensor positions in dense-array EEG. Clin. Neurophysiol. 116, 1130–1140. https://doi.org/10.1016/j.clinph.2004.12.022.
Siems, M., Pape, A.A., Hipp, J.F., Siegel, M., 2016. Measuring the cortical correlation structure of spontaneous oscillatory activity with EEG and MEG. Neuroimage 129, 345–355. https://doi.org/10.1016/j.neuroimage.2016.01.055.
Tagliazucchi, E., Laufs, H., 2014. Decoding wakefulness levels from typical fMRI resting-state data reveals reliable drifts between wakefulness and sleep. Neuron 82, 695–708. https://doi.org/10.1016/j.neuron.2014.03.020.
Tang, W., Liu, H., Douw, L., Kramer, M.A., Eden, U.T., Hämäläinen, M.S., Stufflebeam, S.M., 2017. Dynamic connectivity modulates local activity in the core regions of the default-mode network. Proc. Natl. Acad. Sci. 114, 9713–9718. https://doi.org/10.1073/pnas.1702027114.
Uddin, L.Q., Kelly, A.M.C., Biswal, B.B., Castellanos, F.X., Milham, M.P., 2009. Functional connectivity of Default Mode Network components: correlation, anticorrelation, and causality. Hum. Brain Mapp. 30, 625–637. https://doi.org/10.1002/hbm.20531.
Uhlhaas, P.J., Singer, W., 2010. Abnormal neural oscillations and synchrony in schizophrenia. Nat. Rev. Neurosci. 11, 100–113. https://doi.org/10.1038/nrn2774.
Uhlhaas, P.J., Singer, W., 2006. Neural synchrony in brain disorders: relevance for cognitive dysfunctions and pathophysiology. Neuron 52, 155–168. https://doi.org/10.1016/j.neuron.2006.09.020.
Watrous, A.J., Tandon, N., Connor, C., Pieters, T., Ekstrom, A.D., 2013. Frequency–specific network connectivity increases underlie accurate spatiotemporal memory retrieval. Nat. Neurosci. 16, 349–356. https://doi.org/10.1002/jmri.24785.Free-Breathing.
Wayne, D.W., 1990. Spearman rank correlation coefficient. In: Applied Nonparametric Statistics.
Wolters, C.H., Grasedyck, L., Anwander, A., Hackbusch, W., 2004. Efficient computation of lead field bases and influence matrix for the FEM-based EEG and MEG inverse problem. Inverse Probl. 20, 3–6.
Yao, D., 2001. A method to standardize a reference of scalp EEG recordings to apoint at infinity. Physiol. Meas. 22, 693–711.
Yao, D., Wang, L., Oostenveld, R., Nielsen, K.D., Arendt-Nielsen, L., Chen, A.C.N., 2005. A comparative study of different references for EEG spectral mapping: the issue of the neutral reference and the use of the infinity reference. Physiol. Meas. 26, 173–184. https://doi.org/10.1088/0967-3334/26/3/003.
Yuan, H., Ding, L., Zhu, M., Zotev, V., Phillips, R., Bodurka, J., 2016. Reconstructing large-scale brain resting-state networks from high-resolution EEG: spatial and temporal comparisons with fMRI. Brain Connect. 6, 122–135. https://doi.org/10.1089/brain.2014.0336.
Zhang, S., Tian, S., Chattun, M.R., Tang, H., Yan, R., Bi, K., Yao, Z., Lu, Q., 2018. A supplementary functional connectivity microstate attached to the default mode network in depression revealed by resting-state magnetoencephalography. Prog. Neuro Psychopharmacol. Biol. Psychiatr. 83, 76–85. https://doi.org/10.1016/j.pnpbp.2018.01.006.